Line and band emission from tungsten ions with charge 21+ to 45+ in the 45–70-Å range

R. Radtke and C. Biedermann
Max-Planck-Institut für Plasmaphysik, Bereich Plasmadiagnostik, EURATOM Association, D-10117 Berlin, Germany

J. L. Schwob, P. Mandelbaum, and R. Doron
Racah Institute of Physics, The Hebrew University, 91904 Jerusalem, Israel

(Received 24 July 2000; revised manuscript received 9 January 2001; published 15 June 2001)

We have measured the radiation from medium-charge-state ions of tungsten in the spectral range from 45 to 70 Å. The ions were produced in an electron beam ion trap (EBIT), and the radiation was observed using a 2-m grazing-incidence spectrometer. Operating EBIT with beam energies between 500 eV and 4 keV allowed us to sample charge states ranging from I-like W^{21+} to Cu-like W^{45+}. Lines of Sr-like through Cu-like tungsten were observed; for the Sr-like to As-like ions new lines were identified. Analysis of the spectra is based on *ab initio* calculations using the relativistic HULLAC code. For charge states lower than Sr-like W^{36+}, the spectrum lines fuse into a bright emission band situated around 50 Å. The band extends over an interval of approximately 2 Å and moves smoothly towards shorter wavelengths with decreasing ion-charge state. The shift and narrowing of the band emission cannot be interpreted in the framework of the standard unresolved transition array formalism assuming statistical population of the excited levels. Instead, the observations are explained by detailed calculations based on a collisional-radiative model. It is shown that the variation of the experimental spectrum with charge state is the signature of the low electron density in EBIT.

DOI: 10.1103/PhysRevA.64.012720 PACS number(s): 34.80.Lx, 34.80.Kw, 34.80.Dp, 52.25.Os

I. INTRODUCTION

The short-wavelength spectrum from tungsten ions with unfilled $4d$ and $4f$ subshells in the ground-state configuration has attracted much attention. The reason is that the spectra from such ions, like the spectra from rare-earth and heavier elements in corresponding isoelectronic states, exhibit a remarkable feature. Instead of consisting of a large number of individual lines, they are characterized by bright emission bands appearing between 40 and 70 Å. As suggested in Ref. [1], the quasicontinuum bands are formed by a large number of unresolved spectral lines, originating from mostly $\Delta n=0$ transitions within the $n=4$ shell, though $\Delta n=1$ transitions are also known to create quasicontinuum bands [2,3]. Bands were observed in tokamak plasmas where tungsten occurred as an intrinsic impurity [1,4] or was injected in controlled amounts by laser-ablation techniques [3,5]. A separate effort [6–8] focused on the brightest structure in the tungsten impurity spectrum from tokamak-produced plasmas, the band at 50 Å. The emphasis there was on using high-resolution measurements to reach firmer conclusions about the charge state and the transitions responsible for the particular emission band in question.

The interpretation of the emission bands in terms of atomic physics parameters is the subject of several papers [1,3,9–11]. Using a refined unresolved transition array (UTA) formalism that includes configuration mixing, computations were made in Refs. [9,10] for ionized rare-earth elements having open $4d$ subshells in the ground configuration. For these ions, it was demonstrated that the emission bands originate from resonance transitions of the type $4p^6\,4d^n$-$4p^6\,4d^{n-1}\,4f$ and $4p^6\,4d^n$-$4p^5\,4d^{n+1}$. Most importantly, the calculations revealed that the mixing between the $4p^5\,4d^{n+1}$ and $4p^6\,4d^{n-1}\,4f$ configurations is responsible for the narrowing and the superposition of transition arrays from different ionization stages. A preliminary set of calculations has already been made to predict the mean wavelength and the spectral width of the transition arrays in tungsten [11]. The main result of this calculation is that the arrays remain concentrated in a relatively small wavelength range throughout a sequence of as many as 20 ionization stages.

The importance of tungsten to many modern high-temperature plasma devices has induced new activity to measure the radiation from such ions. This is in addition to the purely spectroscopic interest inherent in this kind of research. Fusion devices constitute a prime example, where the specific characteristics of tungsten make it an important material for various structural components. Recent work has suggested that tungsten may be the best solution for reducing the divertor tile erosion in a fusion reactor [12,13]. Moreover, in a high-recycling divertor with relatively low temperature and high density tungsten has excellent redeposition properties with the result that production of higher ionization stages and associated problems of self-sputtering are in large part suppressed. On the other hand, if sputtered tungsten nonetheless penetrates into the central plasma region it can exist there in various ionization stages, which depend on electron temperature, and has the effect of raising the radiation losses. The radiation from tungsten represents a serious limitation to the energy confinement in a fusion reactor and could quench the fusion reaction if the relative concentration of W ions in the core plasma is higher than about 10^{-5} [14]. Knowledge of the ionization stages and the transitions giving rise to line emission is thus crucial to future design considerations, specifically in estimating the radiated power.

In the present measurements, we used an electron beam ion trap (EBIT) to produce tungsten ions and confine them for spectroscopic observations. EBIT operates with electron densities in the range $n_e \leqslant 10^{13}$ cm^{-3} and as in tokamak

plasmas the confined ions are in a state far from local thermodynamic equilibrium (LTE) that is characterized by a Boltzmann distribution for the level populations. For this reason, our analysis of the radiation from the ions in EBIT relies on collisional-radiative (CR) line intensities that are calculated *ab initio* using the multiconfiguration relativistic Hebrew University Lawrence Livermore Atomic Code (HULLAC) package [15,16]. As demonstrated below, the use of CR line intensities allows the construction of synthetic spectra that show remarkable qualitative agreement with our measurements.

II. EXPERIMENTAL METHOD

Our measurements were performed at the Berlin electron beam ion trap facility and made use of EBIT's capability to control an ion's charge-state distribution by varying the energy of the ionizing electron beam. The electron beam in EBIT originates from an electron gun and is formed by accelerating and guiding electrons into the trap, a region of high magnetic field roughly 2 cm in length. In the 3 T magnetic field of the Berlin EBIT, the beam is compressed to a diameter of about 70 μm. The actual trap consists of three drift tubes; the central one is biased negatively with respect to the end segments, thus creating a potential well that confines the ions in the axial direction. Radial confinement is achieved by a combination of the electrostatic attraction of the electron beam and the axial magnetic field. In addition to trapping the ions, the electron beam also serves to excite them.

In the present experiment, we have followed a particular procedure to generate the tungsten ions and store them in the trap. If desired other elements may also be introduced into EBIT (e.g., by injection in gaseous form), but this requires a different method of preparation. In the procedure used here EBIT's operating parameters (beam-accelerating voltage U_b, electron-beam current I_e, and the axial potential well U_{axial}) were first set to the desired values. Low-charged tungsten ions were then produced by a metal vapor vacuum arc and injected into EBIT. The arc, firing every 5 s, was operated with an extraction voltage U_{extr} higher than the voltage applied to the outer drift tubes ($U_{extr} > U_b + U_{axial}$). Extracted ions then pass the drift-tube assembly without being trapped. They continue to travel down the EBIT axis, and when they hit the cathode of EBIT's electron gun, self-sputtering of tungsten starts; it works very efficiently at an extraction voltage of 5–7 kV resulting in a sputtering yield in the range of 3–4 [17]. Although sputtered tungsten atoms are ionized in the electron beam as they travel towards the drift-tube assembly, at the position of the trap there still remain enough neutral atoms to be trapped after an ionizing collision. In this way, the cathode of the electron gun acts as a source of neutral W atoms, and tungsten ions can concentrate in the trap during extended accumulation. Under conditions present in this experiment, an equilibrium in the photon flux was reached in less than 300 s.

The radiation from the ions in EBIT is observed using a newly developed, interferometrically aligned 2-m Schwob-Fraenkel grazing-incidence spectrometer. The spectrometer, covering the total range of 10–1000 Å, was specially designed and constructed at the Hebrew University for measurements with an EBIT. In the present experiment, the instrument was equipped with a 600 lines/mm grating set at a grazing angle of incidence of 2°. This grating allowed us to view the spectrum between 45 and 70 Å at a single wavelength setting of the detector carriage. Using a 6-m grazing mirror, a one-to-one image of the emitting ions within EBIT is formed on the entrance slit of the spectrometer. In order to take full advantage of the spectrometer resolution a 18 μm wide slit was chosen. The spectra were recorded with a two-stage microchannel plate/phosphor screen image-intensifier system that was fiber-optically coupled to a thermoelectrically-cooled charge-coupled-device (CCD) camera. Using the 18 μm slit, the instrumental full-width-at-half-maximum (FWHM) is approximately 0.2 Å in the 50–100-Å spectral range. *In situ* wavelength calibration of the spectrometer was performed using second-order H-like and He-like lines from nitrogen that was injected into EBIT. Wavelength values were taken from Refs. [18,19].

Spectra were measured for more than 50 separate electron-beam energies, ranging from 500 eV to 4 keV. Operating at these energies allowed us to observe more than 20 different ions ranging from iodine- to copper-like tungsten, W^{21+} to W^{45+}. The ions were sampled using voltage increments of about 50 V, which is comparable to the energy spread of EBIT's electron beam (30–60 eV FWHM depending on the beam current). The electron-beam energy E_{beam} was deduced from the beam-accelerating voltage U_b applied to the drift tube. Corrections were added to account for the effect of the electron and ion space-charge potentials [20]. The error in E_{beam} associated with these corrections is estimated to be ± 20 eV. The electron-beam current was limited throughout these measurements to 50 mA or lower, and each spectrum had an exposure time of about 1 h.

III. LINE SPECTRA

We present in the following a survey of our spectroscopic measurements. Figure 1 displays CCD images showing tungsten spectra in the range 45–70 Å. Each spectrum represents a particular ion population in EBIT corresponding to the indicated electron-beam energy, E_{beam}. The charge number of the highest possible ionization stage was found by comparing the value specified for E_{beam} to the ionization energies $E_I(q)$ for the different charge-state ions. [Values of $E_I(q)$ are taken from calculations performed with the HULLAC package; for the ions with charge $q = 29$–41, these values are listed in Tables I and III].

As one lowers the beam energy from higher values down towards 1.70 keV, many line features appear in the spectra that represent resonance transitions in Cu-like through Sr-like tungsten. Identification of the lines is based on HULLAC calculations and EBIT's capability to vary the beam energy across the ionization thresholds and excite spectra of successive charge states. For beam energies between 4.06 and 2.42 keV, there are several observed lines: 62.32 Å (W^{45+}), 60.87 Å (W^{44+}), 47.69 Å, 60.61 Å, and 61.29 Å (W^{43+}); and last 46.97 Å and 61.30 Å (W^{42+}). These lines repre-

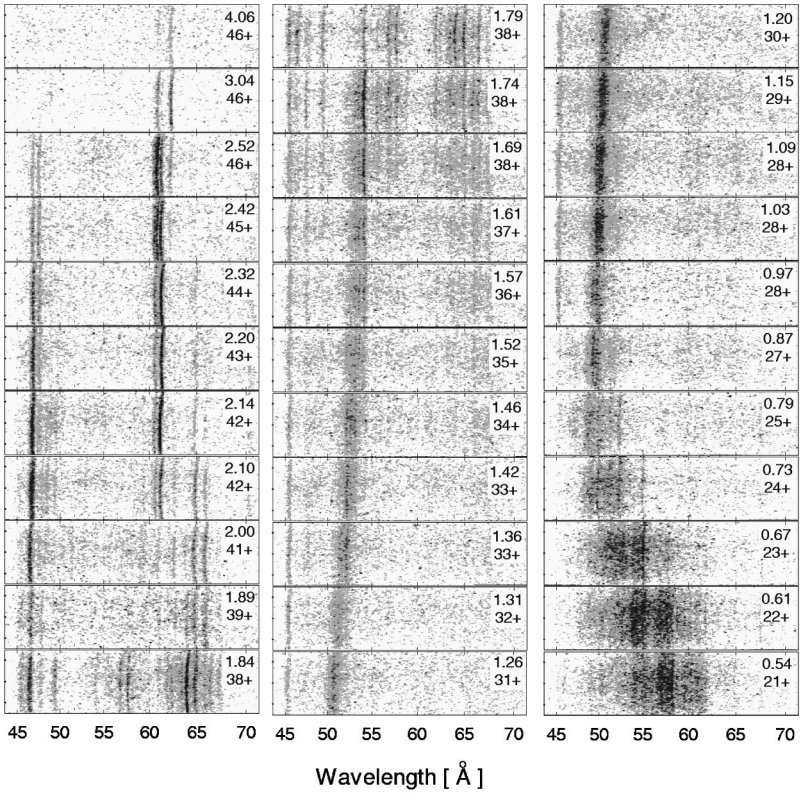

FIG. 1. Spectra from medium-charge-state ions of tungsten between 45 and 70 Å. The upper and lower labels plotted on the right side of each spectrum indicate the energy of the ionizing electron beam (in keV) and the highest allowed charge state of tungsten corresponding to the given value of E_{beam}.

sent $4s$-$4p$ or $4p$-$4d$ resonance transitions in Cu-like through Ge-like tungsten and are known from previous experimental and theoretical work (see for example [21,5,22]). As the beam energy decreases progressively, the ion population in EBIT is shifted to lower charge states. For the sequence following the 2.42-keV spectrum, we observe a weakening of the Ga-like and Ge-like resonance lines in a manner that indicates the absence of these ions for beam energies below about 2 keV. Most prominent in this range of beam energies is the feature situated around 46 Å. It is clearly wider than expected for a single line and moves towards shorter wavelengths as E_{beam} decreases. We could not resolve this feature well enough to identify individual lines, but from our structure calculations we infer that it incorporates contributions from resonance transitions in As-like W^{41+}, Se-like W^{40+}, and Br-like W^{39+}. Besides this complex blend of lines, we could discern several other resonance lines belonging to these ionization states (see Table I). For the beam energies 1.84 and 1.79 keV, the most abundant tungsten ions in the trap are Kr-like W^{38+} and Rb-like W^{37+}. We have measured two new strong lines, which we assign here to resonance transitions in the Kr-like ion, 46.40 Å and 63.98 Å. Note that the latter appears well isolated from other lines. The remaining lines in both of these spectra arise from Rb-like W^{37+} and lower ionization stages. Four Rb-like transitions are presently identified and listed in Table I. The 1.79-keV spectrum shows a strong line at 54.14 Å, which we attribute to Sr-like tungsten. It becomes a prominent feature of the lower energy spectra where it forms the edge of a narrow emission band.

Table I displays the experimental wavelengths of all the tungsten lines observed from the As-like (W^{41+}) through Sr-like (W^{36+}) charge states. The accuracy of the measured wavelengths is ± 0.05 Å. Where available, comparisons are made to observations reported in [5]. In addition, Table I presents the calculated wavelengths and identified transitions. Not listed are the predictions for the wavelengths of these ions made earlier [22]. The method employed there is similar to the present method (both use HULLAC), and the separately computed wavelengths agree to within ± 0.2 Å. One notices in Table I that all of the measured lines appear at somewhat longer wavelengths than predicted. The difference between the measured and calculated wavelengths reaches as much as 1 Å, and it turns out that the wavelengths of the lower charge states are calculated less accurately because of the complexity of the configurations of these ions. Finally, Table I gives the collisional-radiative line intensities (see Sec. IV B) predicted for the electron density and energy in EBIT. Comparison of the calculated and measured intensities helped us to confirm identification of the lines discussed above.

IV. NARROW QUASICONTINUUM BANDS

At electron-beam energies below approximately 1.70 keV, there is a drastic change in qualitative appearance of the spectra as a function of the ion-charge state. A narrow band near 50 Å is emitted along with a weak line at about 45 Å. While the line remains centered at the same position throughout the sequence of spectra, the band shifts towards shorter wavelengths as the charge state decreases. This trend continues until the beam energy becomes less than about 1 keV. Thereafter, the emission pattern disperses and shifts back to higher wavelengths. This starts at the point where

TABLE I. Observed and calculated transitions of As-like through Sr-like tungsten ions. λ_{expt} and λ_{th}, respectively, denote the experimental and theoretical transition wavelengths obtained in the present work. The column λ^{*}_{expt} gives the experimental wavelengths from Ref. [5]. Wavelengths are in angstroms. b indicates that the line is blended with others. I_{CR} is the calculated collisional-radiative line intensity (in 10^2 photons/s per ion) for an electron density $n_e=10^{12}$ cm^{-3} and an electron energy $E=E_I$, where E_I is the ionization energy. For the upper level of each transition, the most important component of the eigenvector is given, preceded by the square of its coefficient. J_L and J_U are the total angular momenta of the lower and upper levels, respectively.

Ion	λ_{expt}	λ^{*}_{expt}	λ_{th}	I_{CR}	Lower level	J_L	Upper level	J_U
As-like W^{41+}	47.16 b	46.9 b	46.69	4.9	$4s^2\,4p_{1/2}^2\,4p_{3/2}$	3/2	73% $4s^2(4p_{1/2}\,4p_{3/2})_2\,4d_{3/2}$	3/2
($E_I=1.99$ keV)	47.16 b	46.9 b	46.64	2.0	$4s^2\,4p_{1/2}^2\,4p_{3/2}$	3/2	88% $4s^2(4p_{1/2}\,4p_{3/2})_2\,4d_{3/2}$	1/2
	47.16 b	46.9 b	47.07	5.7	$4s^2\,4p_{1/2}^2\,4p_{3/2}$	3/2	39% $4s^2(4p_{1/2}\,4p_{3/2})_1\,4d_{3/2}$	5/2
	60.71	60.6	60.26	2.9	$4s^2\,4p_{1/2}^2\,4p_{3/2}$	3/2	85% $4s\,4p_{1/2}^2(4p_{3/2}^2)_2$	3/2
	64.82	64.9	64.69	3.1	$4s^2\,4p_{1/2}^2\,4p_{3/2}$	3/2	61% $4s\,4p_{1/2}^2(4p_{3/2}^2)_2$	5/2
	70.15		69.96	1.5	$4s^2\,4p_{1/2}^2\,4p_{3/2}$	3/2	63% $4s^2\,4p_{1/2}^2\,4d_{5/2}$	5/2
Se-like W^{40+}	46.88 b	46.9 b	46.30	1.6	$4s^2\,4p_{1/2}^2\,4p_{3/2}^2$	0	78% $(4s^2\,4p_{1/2}(4p_{3/2}^2)_0)_{1/2}\,4d_{3/2}$	1
($E_I=1.94$ keV)	46.88 b	46.9 b	46.09	2.6	$4s^2\,4p_{1/2}^2\,4p_{3/2}^2$	2	75% $(4s^2\,4p_{1/2}(4p_{3/2}^2)_2)_{5/2}\,4d_{3/2}$	1
	46.88 b	46.9 b	46.30	3.6	$4s^2\,4p_{1/2}^2\,4p_{3/2}^2$	2	67% $(4s^2\,4p_{1/2}(4p_{3/2}^2)_2)_{5/2}\,4d_{3/2}$	2
	46.88 b	46.9 b	46.34	4.8	$4s^2\,4p_{1/2}^2\,4p_{3/2}^2$	2	50% $(4s^2\,4p_{1/2}(4p_{3/2}^2)_2)_{3/2}\,4d_{3/2}$	3
	62.60		62.34	2.7	$4s^2\,4p_{1/2}^2\,4p_{3/2}^2$	2	69% $4s\,4p_{1/2}^2\,4p_{3/2}^3$	2
	65.81 b	65.8 b	64.79	4.9	$4s^2\,4p_{1/2}^2\,4p_{3/2}^2$	2	89% $4s^2\,4p_{1/2}^2\,4p_{3/2}\,4d_{5/2}$	3
Br-like W^{39+}	46.81 b	46.9 b	46.46	4.8	$4s^2\,4p_{1/2}^2\,4p_{3/2}^3$	3/2	77% $4s^2(4p_{1/2}\,4p_{3/2}^3)_2\,4d_{3/2}$	1/2
($E_I=1.88$ keV)	46.81 b	46.9 b	46.63	4.9	$4s^2\,4p_{1/2}^2\,4p_{3/2}^3$	3/2	41% $4s^2(4p_{1/2}\,4p_{3/2}^3)_2\,4d_{3/2}$	3/2
	46.81 b	46.9 b	46.64	9.4	$4s^2\,4p_{1/2}^2\,4p_{3/2}^3$	3/2	47% $4s^2(4p_{1/2}\,4p_{3/2}^3)_2\,4d_{3/2}$	5/2
	64.74	64.6	64.69	11.0	$4s^2\,4p_{1/2}^2\,4p_{3/2}^3$	3/2	70% $4s^2(4p_{1/2}^2\,4p_{3/2}^2)_2\,4d_{5/2}$	5/2
	65.76 b	65.8 b	65.69	5.9	$4s^2\,4p_{1/2}^2\,4p_{3/2}^3$	3/2	66% $4s^2(4p_{1/2}^2\,4p_{3/2}^2)_2\,4d_{5/2}$	3/2
Kr-like W^{38+}	46.40 b		46.06	26.0	$4s^2\,4p^6$	0	92% $4s^2\,4p_{1/2}^5\,4d_{3/2}$	1
($E_I=1.83$ keV)	63.98		63.25	24.0	$4s^2\,4p^6$	0	85% $4s^2\,4p_{3/2}^5\,4d_{5/2}$	1
Rb-like W^{37+}	49.52		49.06	8.8	$4s^2\,4p^6\,4d_{3/2}$	3/2	82% $4s^2\,4p_{1/2}^5(4d_{3/2}^2)_2$	5/2
($E_I=1.62$ keV)	56.86		56.04	4.8	$4s^2\,4p^6\,4d_{3/2}$	3/2	53% $4s^2\,4p^6\,4f_{5/2}$	5/2
	57.74		56.72	1.8	$4s^2\,4p^6\,4d_{3/2}$	3/2	40% $4s^2\,4p_{3/2}^5(4d_{5/2}^2)_4$	5/2
	64.82		63.87	5.3	$4s^2\,4p^6\,4d_{3/2}$	3/2	59% $4s^2(4p_{3/2}^5\,4d_{3/2})_3\,4d_{5/2}$	3/2
Sr-like W^{36+} ($E_I=1.57$ keV)	54.14		53.21	16.1	$4s^2\,4p^6\,4d_{3/2}^2$	2	69% $4s^2\,4p^6\,4d_{3/2}\,4f_{5/2}$	3

ions with several $4f$ electrons in the ground-state configuration play an important role in the emission of tungsten. Hence, the narrow band emission originates from ions that have either an open $4d$ subshell or a few electrons in the $4f$ subshell.

In the following we give a theoretical analysis of the tungsten spectra using the unresolved transition array scheme. Although spectra for many more charge states were recorded in the present experimental study, the emphasis here is on the ions with $4d^n$ configurations in the ground state. These ions clearly show the narrowing and shift of the band emission and in our view are a suitable test case for theoretical modeling of the spectrum. A discussion of the tungsten bands of the states with even lower charge will be the subject of a forthcoming study.

A. UTA calculations

In this section we will deal with our initial calculations using the basic UTA approach as described previously [9–11,23]. The ions we are considering in the range below 1.70 keV exhibit arrays of spectral lines corresponding to resonance transitions from the $4p^5\,4d^{n+1}$ and $4p^6\,4d^{n-1}\,4f$ excited configurations to the ground configuration $4p^6\,4d^n$. Let E_{ij} represent the set of all individual transition energies belonging to a single array. Then, in the framework of the UTA model [23], one can express the average and the variance of the transition energies, $\overline{E}$ and $\overline{\sigma^2}$, respectively, as the weighted sums

$$\overline{E}=\frac{\sum_{j,i<j} g_j A_{ji} E_{ij}}{\sum_{j,i<j} g_j A_{ji}} \tag{1}$$

and

$$\overline{\sigma^2}=\frac{\sum_{j,i<j} g_j A_{ji} (\overline{E}-E_{ij})^2}{\sum_{j,i<j} g_j A_{ji}}, \tag{2}$$

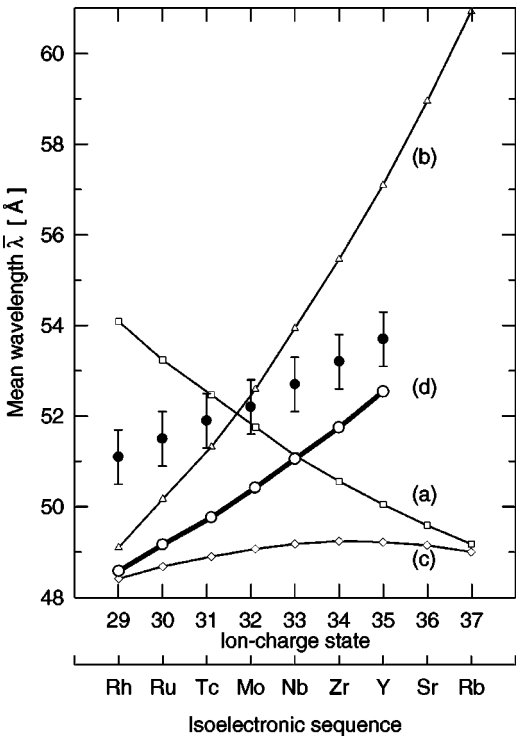

FIG. 2. Mean wavelength for the pure and mixed transition arrays of tungsten as a function of the ion-charge state. Curves (a) and (b) represent the gA-weighted mean wavelength $\overline{\lambda}_{gA}$ for the pure $4p^6\,4d^n-4p^5\,4d^{n+1}$ and $4p^6\,4d^n-4p^6\,4d^{n-1}\,4f$ transition arrays, respectively. Curve (c) shows $\overline{\lambda}_{gA}$ for the mixed $4p^6\,4d^n-[4p^5\,4d^{n+1}+4p^6\,4d^{n-1}\,4f]$ array, visualizing the effect of the configuration interaction. Curve (d) represents the *intensity*-weighted mean wavelength $\overline{\lambda}_{CR}$ for the mixed transition array. The calculation of $\overline{\lambda}_{CR}$ is based on the collisional-radiative line intensities deduced from Eq. (5); the electron density and energy for which Eq. (5) was solved are given in Table III. The solid data circles are from the present EBIT experiment.

where A_{ji} is the Einstein coefficient for spontaneous emission from level j to level i and g_j is the statistical weight of the upper level. Using $\overline{E}$ and $\overline{\sigma^2}$, the mean wavelength $\overline{\lambda}_{gA}$ and the spectral width $\Delta\lambda_{gA}$ of the transition array can be defined as follows

$$\overline{\lambda}_{gA}=10^8/\overline{E}, \tag{3}$$

$$\Delta\lambda_{gA}=\sqrt{8\ln 2}\times 10^8\overline{\sigma}/\overline{E}^2, \tag{4}$$

$\overline{E}$ and $\overline{\sigma}$ are here expressed in cm^{-1} and $\overline{\lambda}_{gA}$ and $\Delta\lambda_{gA}$ in angstroms.

Using Eqs. (1)–(4) as a basis, we have made full intermediate coupling calculations to obtain the UTA parameters for the pure $4p^6\,4d^n-4p^5\,4d^{n+1}$ and $4p^6\,4d^n-4p^6\,4d^{n-1}\,4f$ as well as mixed $4p^6\,4d^n-[4p^5\,4d^{n+1}+4p^6\,4d^{n-1}\,4f]$ transition arrays $(n=1-9)$ of tungsten. Curves (a), (b), and (c) in Fig. 2 and Table II summarize the results of these calculations. Previous UTA calculations [11] for some of these ions have already predicted transition arrays in the spectral region between 46 and 51 Å. However, comparison of the results in terms of mean wavelengths and spectral widths is difficult because only a few of the UTA parameters were actually given in that preliminary study. The present results in Fig. 2 show that for the pure arrays [curves (a) and (b)] $\overline{\lambda}_{gA}$ varies strongly with the charge state, while for the mixed arrays [curve (c)] the variation is very weak, less than 1 Å. Moreover, as listed in Table II, the array width is clearly reduced due to the configuration mixing as in Ref. [9]. As an example, in Fig. 3 we have plotted the actual gA distributions for the pure and mixed transition arrays of Nb-like W^{33+}, showing that the narrowing of the mixed array is primarily due to quenching of the long-wavelength transitions from the $4p^5\,4d^6$ configuration. However, from Fig. 3 it is clear that even the mixed-configuration approximation [curve (c)] cannot predict the very narrow emission bands ($\Delta\lambda_{exp}\leqslant 2$ Å) observed in our experimental spectra. Finally, not only the array width deviates from the measurements, but the presently calculated $\overline{\lambda}_{gA}$ do as well. For example, the 1–1.5-keV-energy spectra of Fig. 1 reveal a displacement of the transition wavelengths near 50 Å by as much as 4 Å. The calculations for the associated charge states [curve (c) in Fig. 2] instead predict an almost constant value for $\overline{\lambda}_{gA}$. Thus, we cannot match $\overline{\lambda}_{gA}$ to the experimental data even if we add an offset of 1–2 Å to the calculated wavelengths corresponding to the error limit for this type of transition [9].

TABLE II. Calculated gA-weighted mean wavelength $\overline{\lambda}_{gA}$ and array width $\Delta\lambda_{gA}$ for the pure and mixed transition array of each ion from Rb-like W^{37+} through Rh-like W^{29+}. The calculations are based on the UTA expressions Eqs. (1) and (2). Wavelengths are given in angstroms.

Ion	Ground-state configuration	$4d$-$4p$		$4f$-$4d$		Mixed	
		$\overline{\lambda}_{gA}$	$\Delta\lambda_{gA}$	$\overline{\lambda}_{gA}$	$\Delta\lambda_{gA}$	$\overline{\lambda}_{gA}$	$\Delta\lambda_{gA}$
Rb-like W^{37+}	$4d$	49.18	14.28	60.93	5.15	49.00	13.16
Sr-like W^{36+}	$4d^2$	49.59	15.09	58.95	5.98	49.15	12.58
Y-like W^{35+}	$4d^3$	50.06	15.71	57.10	6.22	49.22	11.87
Zr-like W^{34+}	$4d^4$	50.56	16.32	55.46	6.15	49.24	10.93
Nb-like W^{33+}	$4d^5$	51.13	16.86	53.94	5.89	49.18	9.84
Mo-like W^{32+}	$4d^6$	51.76	17.40	52.59	5.46	49.07	8.64
Tc-like W^{31+}	$4d^7$	52.47	17.87	51.32	4.92	48.90	7.32
Ru-like W^{30+}	$4d^8$	53.24	18.32	50.17	4.22	48.68	5.89
Rh-like W^{29+}	$4d^9$	54.09	18.68	49.10	3.34	48.41	4.26

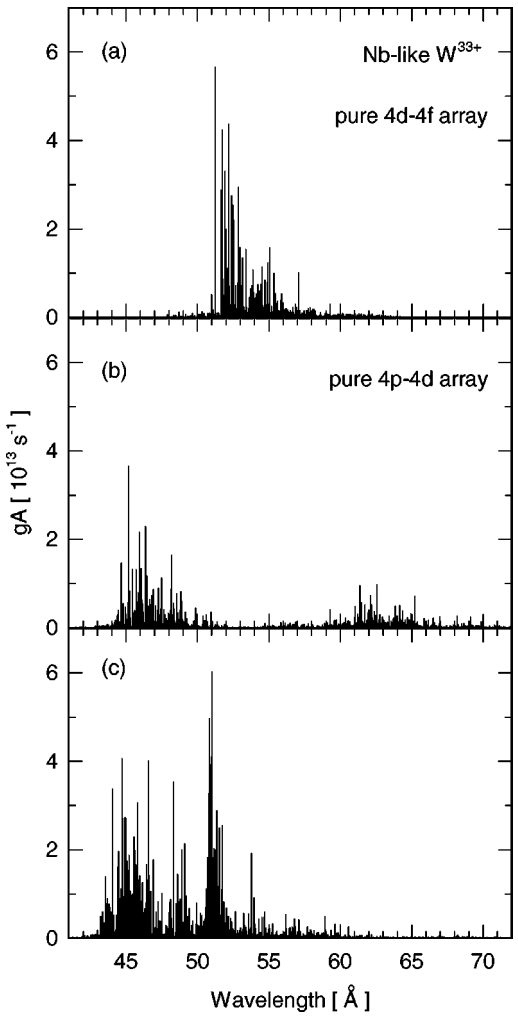

FIG. 3. gA distributions for transitions in Nb-like W^{33+}. In (a) and (b), the distributions for the pure $4p^6\,4d^5-4p^6\,4d^4\,4f$ and $4p^6\,4d^5-4p^5\,4d^6$ transition arrays are presented. (c) is a plot of the gA distribution for the mixed $4p^6\,4d^5-[4p^5\,4d^6+4p^6\,4d^4\,4f]$ array.

B. Density-dependent CR model

To resolve the question of the disparity between the measured and predicted transition wavelengths, a different set of calculations has been made using collisional-radiative line intensities instead of g_jA_{ji} products. The reason is that EBIT operates in a low-collisional regime where level populations no longer follow Boltzmann's law. Line intensities in this case are not proportional to g_jA_{ji} products, but depend instead on the rates at which ions are excited. A calculation of the spectrum must then be based on a collisional-radiative model. To our knowledge, the impact of possible departures from a Boltzmann level population on the determination of the UTA parameters has not been studied previously. Our analysis provides a quantitative description of the transition from very high electron densities, where local thermodynamic equilibrium holds, to moderate and low densities far from LTE.

The population n_j of an ion in level j is calculated from the steady-state rate equation

$$\sum_{i<j} n_i\, n_e\, \sigma^e_{ij}\, v_e + \sum_{k>j} n_k\,(A_{kj} + n_e\, \sigma^d_{kj}\, v_e) = n_j \left\{ \sum_{i<j} (A_{ji} + n_e\, \sigma^d_{ji}\, v_e) + \sum_{k>j} n_e\, \sigma^e_{jk}\, v_e \right\}, \quad (5)$$

where the left-hand and right-hand sides of the equation represent the processes that populate and depopulate the level j. σ^e_{ij} and σ^d_{ji}, respectively, are the energy-dependent electron-impact cross sections for excitation and deexcitation between levels i and j, and v_e is the electron velocity. In solving Eq. (5), electric as well as magnetic dipole and quadrupole radiative decays are taken into account. Once n_j is obtained the line intensity I_{ji}, which represents the number of radiative transitions per second and unit volume from the level j to the level i, is computed using

$$I_{ji} = n_j\, A_{ji}\,. \quad (6)$$

We have generated synthetic spectra for the range $n_e = 10^{12}$–10^{22} cm^{-3}. In addition, the average and the variance of the transition energies have been calculated for the pure and mixed arrays as a function of the electron density. The expressions for $\overline{E}$ and $\overline{\sigma^2}$ in this case are similar to Eqs. (1) and (2), but contain CR line intensities I_{ji} in place of g_jA_{ji} products,

$$\overline{E} = \frac{\sum_{j,i<j} I_{ji}\, E_{ij}}{\sum_{j,i<j} I_{ji}}, \quad (7)$$

$$\overline{\sigma^2} = \frac{\sum_{j,i<j} I_{ji}\,(\overline{E} - E_{ij})^2}{\sum_{j,i<j} I_{ji}}. \quad (8)$$

The UTA parameters expressed now in terms of CR line intensities are designated by $\overline{\lambda}_{CR}$ and $\Delta\lambda_{CR}$; their values were calculated using Eqs. (7) and (8).

A representative plot of CR spectra for the pure and mixed transition arrays of Nb-like W^{33+} is shown in Figs. 4(a)–4(c). If we compare them to the corresponding gA distributions of Fig. 3, large changes are apparent in the CR spectra. Most noticeably a comparatively small fraction of the transitions within the array have sufficiently high intensity to remain significant in the emission. The predicted mean wavelength for the mixed-transition array of Nb-like W^{33+} is $\overline{\lambda}_{CR} = 51.05$ Å, which clearly differs from the result for the gA distribution $\overline{\lambda}_{gA} = 49.18$ Å. The bottom plot of Fig. 4 shows the CR spectrum for the mixed transition array of Sr-like W^{36+}. Compared to W^{33+}, W^{36+} shows a level structure which is much less complex. As a result, in the spectrum of Sr-like W^{36+} one no longer finds the typical

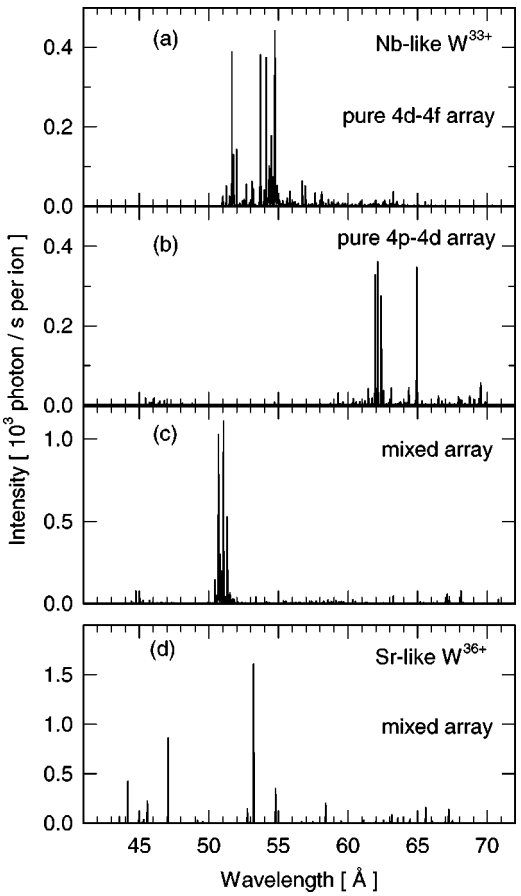

FIG. 4. Collisional-radiative spectra of Nb-like W^{33+} and Sr-like W^{36+}. In (a) and (b), the spectra from the pure $4p^6\,4d^5-4p^6\,4d^4\,4f$ and $4p^6\,4d^5-4p^5\,4d^6$ transition arrays of Nb-like W^{33+} are plotted. (c) and (d) show the spectra for the mixed $4p^6\,4d^n-[4p^5\,4d^{n+1}+4p^6\,4d^{n-1}\,4f]$ array of Nb-like W^{33+} $(n=5)$ and Sr-like W^{36+} $(n=2)$, respectively. All spectra were calculated at an electron density of $n_e=10^{12}$ cm^{-3} and energies of $E=1.38$ keV (for the Nb-like tungsten) and 1.57 keV (for the Sr-like tungsten).

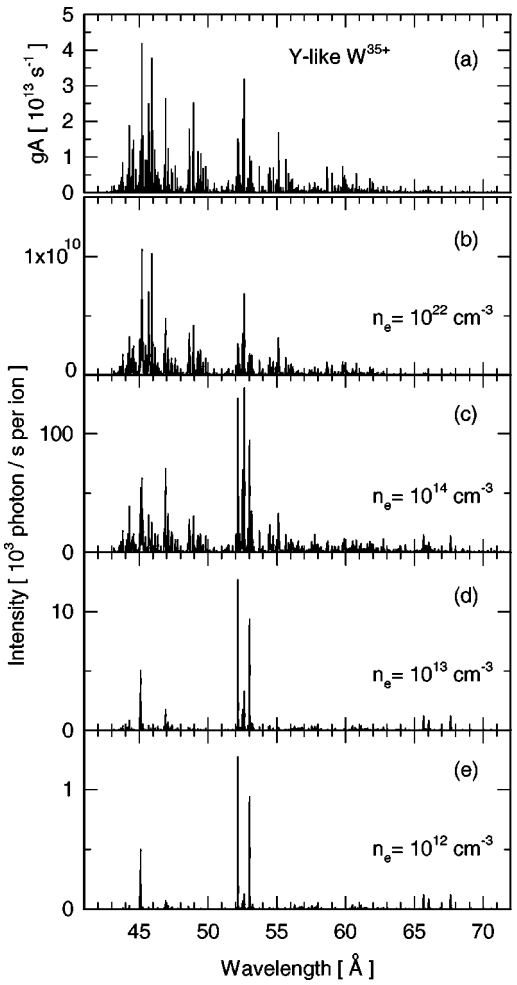

FIG. 5. gA distribution (a) and collisional-radiative spectra for the mixed $4p^6\,4d^3-[4p^5\,4d^4+4p^6\,4d^2\,4f]$ transition array of Y-like W^{35+}. For the spectra plotted in (b) through (e), the electron density changes over ten orders of magnitude from 10^{22} to 10^{12} cm^{-3}. Notice that the intensity of the spectrum lines varies accordingly. Each spectrum is calculated at an electron energy of $E=1.51$ keV.

UTA structure in which lines fuse into a bright emission band.

The effect of the electron density on the intensity distribution is visualized in the plots of Fig. 5 where we present synthetic W^{35+} spectra calculated using the mixed configuration scheme. At the highest electron density (10^{22} cm^{-3}), the general shape of the CR spectrum is very similar to the gA distribution plotted in 5(a). This range is close to the LTE regime, and most of the line intensities approach the values of their corresponding g_jA_{ji} products. At electron densities below about 10^{14} cm^{-3}, one encounters a domain in which the CR spectrum is fundamentally different both from the gA distribution as well as from results obtained at higher densities. As Figs. 5(d) and 5(e) exhibit, the spectrum has split into a single line at approximately 45 Å and a feature at 52.5 Å comprised of a few strong lines. Note that there is no obvious shift of the feature at 52.5 Å as a function of n_e. However, it is displaced from the position of the analogous line group for the W^{33+} ion presented in Fig. 4(c), and the displacement shows the same general variation with charge state as do the emission bands in the experimental spectra.

A systematic set of calculations has thus been made to predict the mean wavelength and the width of the central line group for each ion, from Rh-like W^{29+} through Y-like W^{35+}. Sr-like W^{36+} and Rb-like W^{37+} do not show the typical UTA structure in their spectra, as outlined above, and were excluded from this study. The calculations were made for an electron density of $n_e=10^{12}$ cm^{-3}, which is the approximate electron density in our measurements. Table III lists the results, and one notices that $\overline{\lambda}_{CR}$ increases gradually with increasing charge state. The peak width exhibits a maximum for Mo-like W^{32+} and Nb-like W^{33+}, corresponding to the fact that these ions have the largest number of excited levels among the tungsten ions with $4d^n$ ground configurations. Δ indicates the difference in the mean wavelengths between the gA-weighted and the *intensity*-weighted UTA results. This quantity is small for Rh-like W^{29+}, but increases significantly for Y-like W^{35+}.

TABLE III. *Intensity*-weighted mean wavelength $\overline{\lambda}_{CR}$ and array width $\Delta\lambda_{CR}$ calculated for the mixed-transition array of each ion from Y-like W^{35+} through Rh-like W^{29+}. The calculations are based on the collisional-radiative line intensities deduced from Eq. (5). The electron density and energy for which the UTA parameters of each ion were calculated are $n_e = 10^{12}$ cm^{-3} and $E = E_I$. E_I is the ionization energy. $\overline{\lambda}_{expt}$ is the experimental mean wavelength of the band inferred from the spectra of Fig. 1. $\Delta = \overline{\lambda}_{CR} - \overline{\lambda}_{gA}$ is the difference between the *intensity*-weighted mean wavelength and the gA-weighted mean wavelength of Table III. $\overline{\lambda}_{CR}$, $\overline{\lambda}_{expt}$, $\Delta\lambda_{CR}$, and Δ are given in angstroms.

Ion	E_I(keV)	$\overline{\lambda}_{CR}$	$\overline{\lambda}_{expt}$	$\Delta\lambda_{CR}$	Δ
Y-like W^{35+}	1.51	52.54	53.7	0.41	3.32
Zr-like W^{34+}	1.46	51.75	53.2	0.41	2.51
Nb-like W^{33+}	1.38	51.05	52.7	0.54	1.87
Mo-like W^{32+}	1.33	50.42	52.2	0.56	1.35
Tc-like W^{31+}	1.28	49.76	51.9	0.40	0.86
Ru-like W^{30+}	1.23	49.16	51.5	0.39	0.48
Rh-like W^{29+}	1.18	48.58	51.1	0.19	0.17

C. Comparison with experiment

The values for $\overline{\lambda}_{CR}$ listed in Table III are plotted in Fig. 2 [curve (d)] where they are compared with the results from the present experiment. Obtaining the experimental data points was not a straightforward procedure because, in the low-energy spectra of Fig. 1, we could no longer resolve individual charge states. As a result, there was no easy way to link the changing positions of the emission band to the presence of a particular ionic stage in the trap. To determine the most abundant charge state as a function of beam energy, we relied on the analysis of the higher-energy spectra of Fig. 1, where we could resolve individual ionization stages. The measured line intensities in these spectra vary as a function of E_{beam} and are enhanced considerably when the population of the emitting ion within EBIT is maximal. Such enhancement can be seen in the 1.74-keV-energy spectrum of Fig. 1 where the intensity of the 54.14-Å Sr-like resonance transition reaches its maximum value. Using these measured line intensities, we were able to determine the electron-beam energy at which an ion population reached a peak under the present experimental conditions. For the ions of charge state q between $36+$ and $44+$, a maximum enhancement was observed when the beam energy was roughly 1.1 times the ionization energy of the next lower charge state $q-1$.

Our analysis of the emission bands in Fig. 1 assumes that this factor is also applicable to the lower charge states. We used it here to predict the energies E_q at which the maximum population is expected for each ion q, from Rh-like W^{29+} through Y-like W^{35+}. We then plotted $\overline{\lambda}_{expt}$, the mean wavelength of the experimental emission band, as a function of E_{beam} and used the $\overline{\lambda}_{expt}$-$E_{beam}$ graph to find $\overline{\lambda}_{expt}$ for each value of E_q. The data resulting from this evaluation are presented in Fig. 2 and Table III. The error in $\overline{\lambda}_{expt}$ is estimated to be ± 0.6 Å. It arises from the uncertainty in the energy factor above, the uncertainty in the determination of the electron-beam energy, and the inherent energy spread of EBIT's electron beam.

Figure 2 shows experimentally determined mean wavelengths that exceed the predicted wavelengths [curve (d)] by 1.2–2.5 Å, depending on charge state. The estimated uncertainty in the theoretical values is 1–2 Å, as stated above, and we are aware that for these kinds of transitions our calculations generally produce wavelengths that are too small. Thus, the most important feature to compare with experimental data is the variation of the wavelengths as a function of charge state. As observed in Fig. 2, the slope of the theoretical curve (d) agrees fairly well with the experimental slope. When q decreases the experimental mean wavelengths are seen to diverge slightly from the calculations. It is likely that this difference is related to the problem of finding the charge balance and that an improvement in charge resolution could resolve the discrepancy. Nevertheless, the fact that experimental data points closely follow the $\overline{\lambda}_{CR}$ curve (d) rather than the $\overline{\lambda}_{gA}$ curve (c) is a clear indication that the peculiarities of the experimental tungsten spectrum are due to the low electron density. One also notices that the theoretical width $\Delta\lambda_{CR}$ (see Table III) is always smaller than the experimental bandwidth for any energy value in the range 1–1.7 keV. This is explained by the fact that at the energy at which a given charge state q is dominant there is still a significant contribution from the next lower and higher ionization states. However, as observed in Fig. 2 the band shifts by nearly 0.5 Å in moving from one charge state to the next. Thus, the slightly enlarged bandwidth that is measured results from the superposition of the emissions of all ions with a significant concentration at a fixed beam energy.

V. CONCLUSIONS

With EBIT's capability to selectively produce and excite particular ionic stages we were able to observe the radiation from highly charged tungsten in a wide range of charge states. The present study has led to the measurement and classification of new lines corresponding to transitions within the $n=4$ shell in Sr-like W^{36+} through Cu-like W^{45+}. For the lower ionization states with $4d^n$ configurations in the ground state (from Rb-like W^{35+} through Rh-like W^{29+}) the EBIT spectra have revealed that the emission fuses into a

narrow band near 50 Å . The band moves smoothly towards shorter wavelengths as decreasing charge states are progressively selected. The analysis of this peculiar effect has been supported by *ab initio* calculations using the multiconfiguration relativistic HULLAC package associated with a collisional-radiative model for the level populations. The usual UTA formalism based on statistical level populations is demonstrated to be inadequate for interpreting the EBIT measurements. In contrast, the density-dependent CR model correctly predicts both the narrowness of the bands and the trend of the wavelength shift observed in the experimental spectra. It is shown that this particular shift is a signature of the low-collisional regime prevailing in EBIT.

We have found experimental and theoretical evidence that more than ten ionization stages of tungsten can contribute to the radiation in the narrow range between 48 and 54 Å . Our results explain thus the unresolved *broad* emission feature around 50 Å observed in the impurity spectrum from tokamak-produced plasmas [5] where, in contrast to EBIT, many more ionization states of tungsten emit simultaneously.

[1] R. C. Isler, R. V. Neidigh, and R. D. Cowan, Phys. Lett. **63A**, 295 (1977).

[2] J. L. Schwob, M. Klapisch, N. Schweitzer, M. Finkenthal, C. Breton, C. DeMichelis, and M. Mattioli, Phys. Lett. **62A**, 85 (1977).

[3] M. Finkenthal, L. K. Huang, S. Lippmann, H. W. Moos, P. Mandelbaum, J. L. Schwob, M. Klapisch, and the TEXT Group, Phys. Lett. A **127**, 255 (1988).

[4] E. Hinnov and M. Mattioli, Phys. Lett. **66A**, 109 (1978).

[5] K. Asmussen, K. B. Fournier, J. M. Laming, R. Neu, J. F. Seely, R. Dux, W. Engelhardt, J. C. Fuchs, and the ASDEX Upgrade Team, Nucl. Fusion **38**, 967 (1998).

[6] J. Sugar, V. Kaufman, and W. L. Rowan, J. Opt. Soc. Am. B **10**, 799 (1993).

[7] J. Sugar, V. Kaufman, and W. L. Rowan, J. Opt. Soc. Am. B **10**, 1321 (1993).

[8] J. Sugar, V. Kaufman, and W. L. Rowan, J. Opt. Soc. Am. B **10**, 1977 (1993).

[9] P. Mandelbaum, M. Finkelthal, J. L. Schwob, and M. Klapisch, Phys. Rev. A **35**, 5051 (1987).

[10] J. Bauche, C. Bauche-Arnoult, M. Klapisch, P. Mandelbaum, and J. L. Schwob, J. Phys. B **20**, 1443 (1987).

[11] P. Mandelbaum, J. L. Schwob, M. Finkenthal, and M. Klapisch, J. Phys. Colloq. **49**, Cl-217 (1988).

[12] A. R. Field, G. Fussmann, C. Garcia-Rosales, S. Hirsch, G. Lieder, D. Naujoks, R. Neu, C. S. Pitcher, R. Radtke, U. Wenzel, and the ASDEX Upgrade Team, J. Nucl. Mater. **220-222**, 553 (1995).

[13] D. Naujoks, K. Asmussen, M. Bessenrodt-Weberpals, S. Deschka, R. Dux, W. Engelhardt, A. R. Field, G. Fussmann, J. C. Fuchs, C. Garcia-Rosales, S. Hirsch, P. Ignacz, G. Lieder, K. F. Mast, R. Neu, R. Radtke, J. Roth, U. Wenzel, and the ASDEX Upgrade Team, Nucl. Fusion **36**, 671 (1996).

[14] N. J. Peacock, R. Barnsley, N. C. Hawkes, K. D. Lawson, and M. G. 0'Mullane, in *Diagnostics for Experimental Thermonuclear Fusion Reactors*, edited by P. Stott, G. Giuseppe, and E. Sindoni (Plenum Press, New York, 1996), p. 291.

[15] A. Bar-Shalom, M. Klapisch, and W. H. Goldstein, The HULLAC Code for Atomic Physics (1988) (unpublished).

[16] A. Bar-Shalom, M. Klapisch, and J. Oreg, Phys. Rev. A **38**, 1773 (1988).

[17] W. Eckstein, C. Garcia-Rosales, J. Roth, and W. Ottenberger, *Sputtering Data*, Rep. IPP 9/82, Max-Planck-Institut für Plasmaphysik, Garching (1993).

[18] L. Engström and U. Litzen, J. Phys. B **28**, 2565 (1995).

[19] W. R. Johnson and G. Soff, At. Data Nucl. Data Tables **33**, 405 (1985).

[20] R. Radtke, C. Biedermann, T. Fuchs, and G. Fussmann (unpublished).

[21] J. F. Seely, C. M. Brown, and W. E. Behring, J. Opt. Soc. Am. B **6**, 3 (1989).

[22] K. B. Fournier, At. Data Nucl. Data Tables **68**, 1 (1998).

[23] J. Bauche, C. Bauche-Arnoult, M. Klapisch, Adv. At. Mol. Phys. **23**, 131 (1987).